Original Article
Published: 2025-09-16
https://doi.org/10.6425/022025jept002

Theoretical Investigations of the Properties of Some Dy-Porphyrins

Slaviţa Rotunjanu [1,2]✉, Raluca Pop [1,*]✉, Marius Mioc [1,2]✉, Mihaela Jorgovan [1,2]✉, Elisabeta Atyim [1,2]✉ and Codruţa Şoica [1,2]✉

[1]Faculty of Pharmacy, Victor Babes University of Medicine and Pharmacy, 300041 Timişoara, Romania
[2]Research Center for Experimental Pharmacology and Drug Design (X-Pharm Design), "Victor Babes" University of Medicine and Pharmacy, 300041 Timişoara, Romania
*email: pop.raluca@umft.ro

Abstract

Porphyrins are a class of naturally occurring intensely colored compounds (ranging in color from red to violet) with a macrocyclic structure. Both as free base and containing a central metal (metalloporphyrins), they have found various applications in pharmaceutical and medical fields. One of the most important properties of these compounds is represented by their tunable properties, given the various metals and substituents that can be employed. The present study dealt with the investigation, by means of computational chemistry, of the energetic and geometric properties of a series of proposed Dy(III)-porphyrins. The influence of various substituents grafted off the porphyrin macrocycle is discussed as a function of the calculated properties, like the frontier molecular orbitals energies, molecular area and volume, polarizability, and polar surface area.

Keywords: *dysprosium; metalloporphyrins; Dy(iii)-porphyrins; density functional theory; molecular mechanics*

Citation: Rotunjanu S, Pop R, Mioc M, Jorgovan M, Atyim E, Şoica C. Theoretical Investigations of the Properties of Some Dy-Porphyrins. *Journal of Experimental Pharmacology and Toxicology* 2025;2. https://doi.org/10.6425/022025jept002

1. Introduction

Metalloporphyrins are molecules consisting of a porphyrin ring coordinated with a metal ion, especially a transition metal. The porphyrin structure is represented by four pyrrole rings connected by methyne bridges.

Metalloporphyrins are being investigated as drug carriers, particularly in cancer treatment, due to their unique properties and their potential for targeted drug delivery [1]. They can be incorporated into various nanomaterials, like metal–organic frameworks or nanogels, or used as building blocks for drug delivery systems, leading to a controlled release and enhanced therapeutic efficacy [1]. The main advantages of this class of compounds are their biocompatibility, making them suitable for biomedical applications, and their adjustable properties. The metal ion and porphyrin structure can be modified to tailor the properties of the metalloporphyrin for specific drug delivery needs [2].

A literature survey showed various applications for various substituted metalloporphyrins. Tin-containing metalloporphyrins have been investigated as a potential treatment of neonatal hyperbilirubinemia. They act as inhibitors of the enzyme heme oxygenase, which is responsible for breaking down heme and producing bilirubin. By inhibiting this enzyme, metalloporphyrins can reduce the amount of bilirubin produced, potentially alleviating the severity of hyperbilirubinemia [3, 4].

Molecular imprinting polymers with porphyrins and iron(II)porphyrins have been successfully used for the selective binding of hemoglobin [5]. The synthesized porphyrins were substituted with 4-allyloxyphenyl residues on the methine bridges.

Metalloporphyrins (metal range: Ca-Zn) were investigated as possible drug carriers for fluorouracil by computational chemistry methods. The results showed that the highest affinity was obtained for Ti-porphyrin [6]. Manganese(III) porphyrin complexes have been synthesized and characterized; their antibacterial, antifungal, and antioxidant activity has been investigated [7]. They were effective inhibitors of the Gram-positive strains *S. aureus* and *B. cereus*; also, they present an enhanced sensitivity towards *C. krusei*, sensitivity that increases for the metalloporphyrins compared to the free porphyrins [7].

Another series of free-base porphyrins and metalloporphyrins have been synthesized and evaluated for possible antitumor activity [8]. Good results have been obtained for the free porphyrins and Zn-porphyrins; the positive influence of the substituents has been emphasized for benzene substituted with electron-attracting groups [8].

Metalloporphyrins substituted with benzenesulfonic acid have been synthesized and characterized; metalloporphyrins of three lanthanides (Pr, Eu, and Ce) have been obtained [9]. The porosity and magnetic properties of these compounds make them suitable for gas storage, catalysis, and sensing applications.

Another study investigates the influence of the energy levels of lanthanide ions on the luminescence properties of metalloporphyrins [10]. Specifically, the presence and position of f-orbital energy levels relative to the porphyrin's singlet (S1) and triplet (T1) excited states dictate whether energy transfer occurs, affecting the type and intensity of luminescence observed [8]. The ability to modify the luminescence properties of metalloporphyrins by selecting specific lanthanide ions with specific energy levels is valuable for developing materials with desired optical properties for various applications, including bioimaging and sensing. According to the authors, the choice of lanthanide ion energy levels is important for designing and synthesizing metalloporphyrins with specific optic characteristics.

Another study [11] presents the applications of metalloporphyrins in diagnostic imaging, including MRI (metalloporphyrins can be designed to enhance contrast in MRI scans, improving the visibility of tumors and other tissues); fluorescence imaging (porphyrins can be used as fluorescent probes for bio-imaging applications, enabling the visualization of specific cellular targets); or PET, SPECT, and CT. Porphyrin derivatives can be radiolabeled with various isotopes for use in Positron Emission Tomography (PET), Single-Photon Emission Computed Tomography (SPECT), and Computed Tomography (CT) imaging.

The use of specific nanomaterials in drug delivery systems has significantly advanced cancer therapy by improving both the efficiency and delivery of therapeutic agents. These materials, including nanoparticles, liposomes, and nanogels, have properties such as enhanced drug solubility, protection from degradation, and targeted delivery to tumoral tissues, minimizing side effects on healthy cells. Metal–organic frameworks based on porphyrin can entrap a range of therapeutic agents, resulting in the application of these materials for drug delivery in cancer therapy [12].

The present study aims to investigate the electronic, geometric, and steric properties of 10 Dy(III)-porphyrins, with the general structure depicted in **Figure 1**:

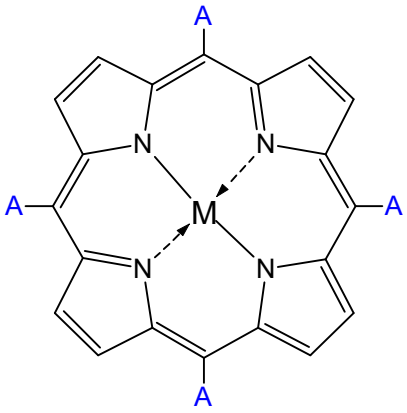

Compound ID:	1	2	3	4	5	6	7	8	9	10
Substituent A:	-H	$-CH_3$	-F	$-CH_2F$	-Cl	$-CH_2Cl$	$-NH_2$	$-CH_2NH_2$	-OH	$-CH_2OH$

Figure 1. General structure of the investigated metalloporphyrins (M = Dy(III)).

A previous work [13] has dealt with the evaluation of some substituted porphyrins with fluorine, hydroxyl, aminoethyl, and hydroxyethyl groups as possible photosensitizers. In this regard, the same substituents have been chosen for our study involving the characterization of dysprosium porphyrins.

2. Materials and Methods

2.1. Computational Details

The molecular structures of Dy-porphyrin complexes (compounds **1**–**10**) were initially optimized by molecular mechanics methods using the Universal Force Field (UFF) implemented in Spartan 14 software (Wavefunction, Inc., Irvine, CA,

USA) [14]. The obtained geometries were subsequently refined by Density Functional Theory (DFT) calculations [14], at the EDF2/6-31+G(d) level of theory using the above-mentioned software package. All calculations were performed in the gas phase, without using symmetry any restrictions. Standard convergence thresholds (maximum displacement < 0.005 Å; maximum gradient < 0.002 Hartree/Bohr) were used for geometry optimizations. Vibrational frequency analyses were conducted in order to confirm that all optimized structures matched true minima (no imaginary frequencies).

The visualization of the frontier molecular orbitals HOMO and LUMO, as well as the extraction of computed electronic parameters (orbital energies, HOMO–LUMO gap, dipole moment, and polarizability), was also performed by means of Spartan 14. Steric parameters such as molecular surface area, molecular volume, ovality, and polar surface area, were also computed with the same software by using built-in descriptors. The measurement of bond lengths between dysprosium and the nitrogen atoms of the porphyrin structures have been performed by using Chem3D software (PerkinElmer Informatics).

3. Results and Discussions

The optimized geometries of the investigated series of compounds have been employed for the calculation of the energetic parameters like the total energy per atom and the HOMO–LUMO gap.

The results presented in **Table 1** summarize the values of the total energy/atom calculated for the metalloporphyrins.

Table 1. Total energy/atom (EDF2/6-31+G(d)).

Compound	General formula	Total energy/atom (a.u.)
1	$C_{20}H_{12}DyN_4$	−27.737
2	$C_{24}H_{20}DyN_4$	−24.152
3	$C_{20}H_8DyN_4F_4$	−38.461
4	$C_{24}H_{16}DyN_4F_4$	−32.249
5	$C_{20}H_8DyN_4Cl_4$	−77.425
6	$C_{24}H_{16}DyN_4Cl_4$	−61.670
7	$C_{20}H_{16}DyN_8$	−27.726
8	$C_{24}H_{24}DyN_8$	−24.643
9	$C_{20}H_{12}DyN_4O_4$	−32.367
10	$C_{24}H_{20}DyN_4O_4$	−28.003

The analysis of the calculated energies/atom shows that the grafted methylene group on the methyne bridges (compounds **2**, **4**, **6**, **8**, and **10**) leads to a decrease in the stability of the proposed metalloporphyrin structures. The aforementioned results also suggest that the presence of a halogen atom (especially chlorine) increases the stability of the compounds. The lowest values were obtained for the methyl-substituted Dy-porphyrin (**2**), followed by the one substituted with the aminomethyl group (**8**).

The influence of the substituents on the investigated metalloporphyrins has also been evaluated by means of the HOMO-LUMO gap. The energy difference between the frontier molecular orbitals is considered a good indicator of the stability/reactivity of a compound: larger HOMO-LUMO gaps suggest an increased stability, while smaller HOMO-LUMO gaps are correlated with enhanced reactivity.

The obtained values of the frontier molecular orbitals, together with the calculated HOMO-LUMO gaps, are depicted in **Table 2**.

According to these results, all the investigated metalloporphyrins are characterized by lower stability. The presence of the substituents strongly influences the value obtained. In general, the presence of -X group on the methyne bridges leads to the obtained of slightly higher HOMO-LUMO gaps, compared to the ones that also have a methylene group, -CH_2X. A single exception occurred, regarding the unsubstituted Dy-porphyrin **1**, that is characterized by a smaller energy gap of the frontier molecular orbitals compared to the methyl-substituted structure **2**.

Table 2. Frontier molecular orbitals energies, together with the calculated HOMO-LUMO gap (EDF2/6-31+G(d)).

Compound	HOMO energy (eV)	LUMO energy (eV)	HOMO-LUMO gap (eV)
1	−15.82	−15.58	0.24
2	−15.15	−14.60	0.55
3	−16.33	−15.67	0.66
4	−15.90	−15.33	0.57
5	−15.72	−15.06	0.66
6	−15.35	−14.80	0.55
7	−15.06	−13.61	1.45
8	−14.43	−14.07	0.36
9	−15.70	−14.60	1.10
10	−15.10	−14.53	0.57

The visualization of HOMO (Highest Occupied Molecular Orbital) and LUMO (Lowest Unoccupied Molecular Orbital) is a key parameter for organic compounds, helping to understand and predict the stability, reactivity, and electronic properties of a molecule. In the field of drug design and pharmaceutical applications, the distribution of the HOMO and LUMO orbitals offer insights regarding the potential interaction sites with biological targets, together with the evaluation of the stability and reactivity of the compounds.

Graphical representation of the frontier molecular orbitals HOMO and LUMO has been performed. The results are presented in **Figure 2**, **Figure 3**, **Figure 4** and **Figure 5** and outline some differences among the studied Dy-porphyrins.

According to the results illustrated in **Figure 2**, **Figure 3**, **Figure 4** and **Figure 5**, the same pattern is encountered in the distribution of the HOMO orbitals for the compounds **1**, **2**, **3**, **5**, **7**, and **9** (the unsubstituted porphyrin and the ones with CH_3, F, NH_2, and OH grafted on the methyne bridge). For these compounds, the HOMO orbitals appear localized mostly on the pyrrole rings. Instead, the porphyrins **4**, **6**, **8**, and **10** (substituted with CH_2X groups) show that the HOMO orbitals are also localized on the methyne group and on the grafted CH_2X moiety. As exception, the porphyrins 7 and 8 (substituted with amino and methyamino groups) are characterized by a lesser delocalization of the HOMO orbitals (on two of the four substituents). This situation is correlated to the lowest values of the HOMO energy computed for compounds **7** and **8**, as depicted in **Table 2**. Instead, the LUMO orbitals are mostly localized on the four methyne bridges and, to a small extent, on the substituents (excepting the compounds **4** and **6**, substituted with CH_2F and CH_2Cl, respectively). The results of LUMO energies presented in **Table 2** show the lower values calculated for compounds **7**–**10**, the ones substituted with amino and hydroxyl groups.

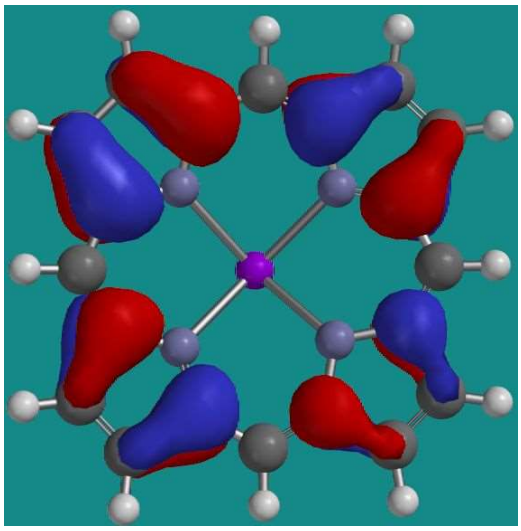

HOMO orbitals of compound **1**

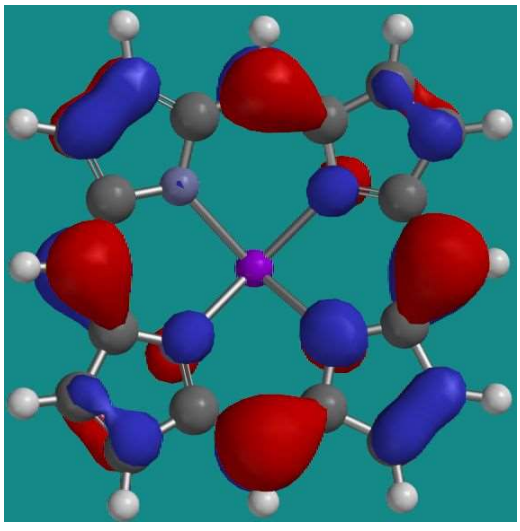

LUMO orbitals of compound **1**

Figure 2. Graphic representation of the frontier molecular orbitals of compound **1**.

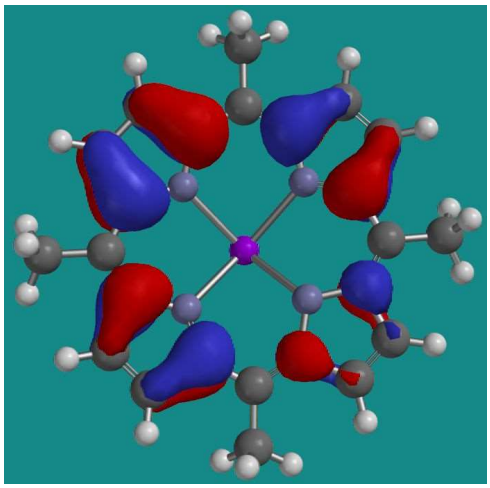

HOMO orbitals of compound **2**

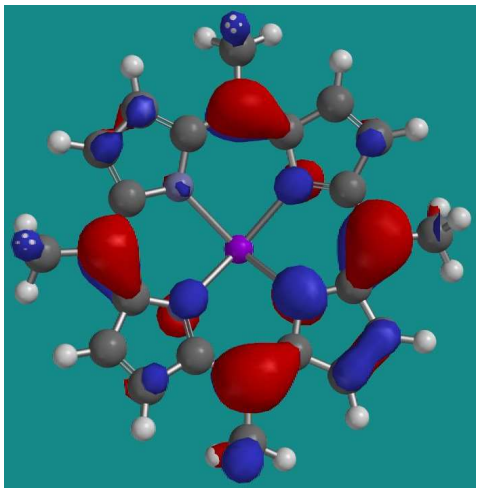

LUMO orbitals of compound **2**

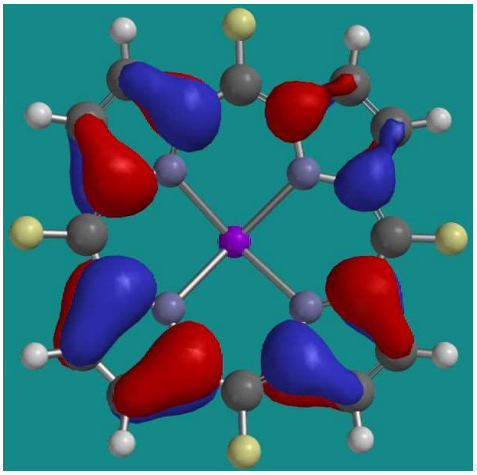

HOMO orbitals of compound **3**

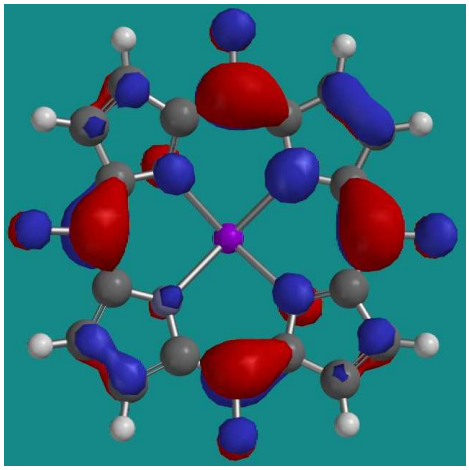

LUMO orbitals of compound **3**

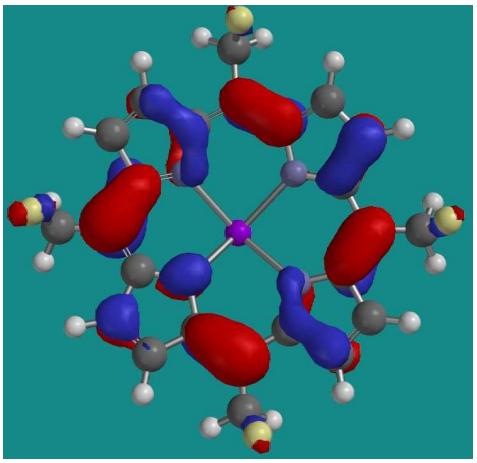

HOMO orbitals of compound **4**

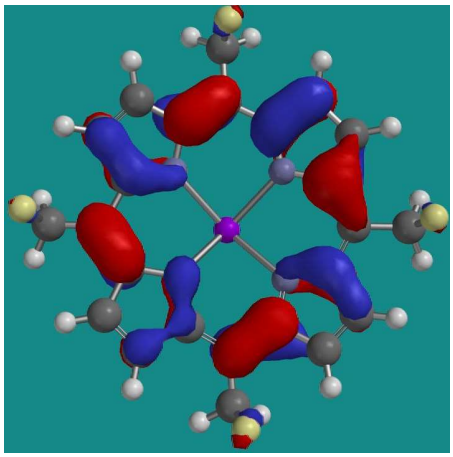

LUMO orbitals of compound **4**

Figure 3. Graphic representation of the frontier molecular orbitals of compounds **2**–**4**.

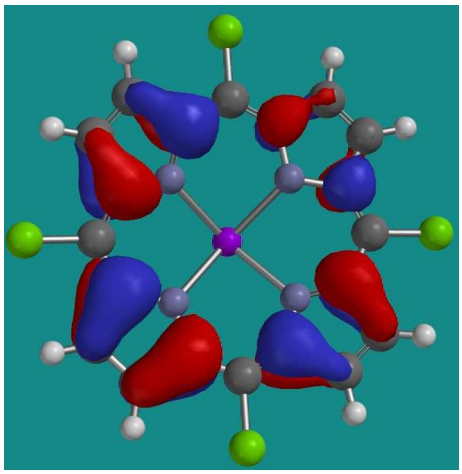

HOMO orbitals of compound **5**

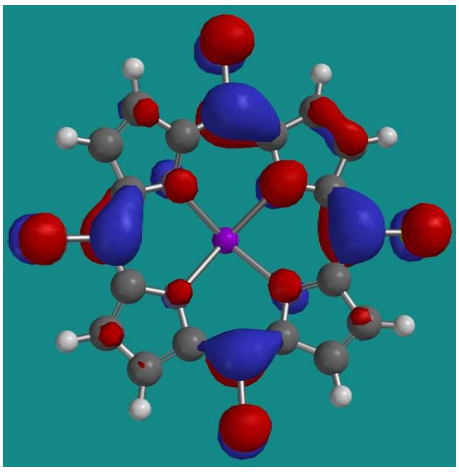

LUMO orbitals of compound **5**

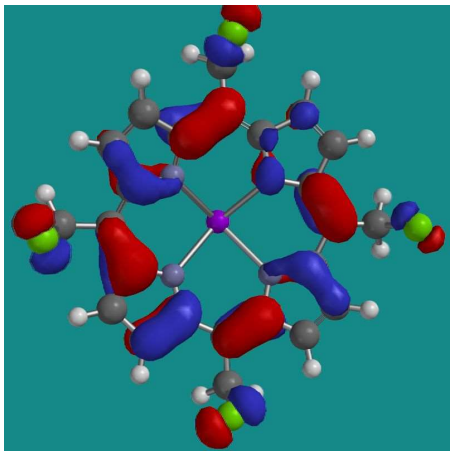

HOMO orbitals of compound **6**

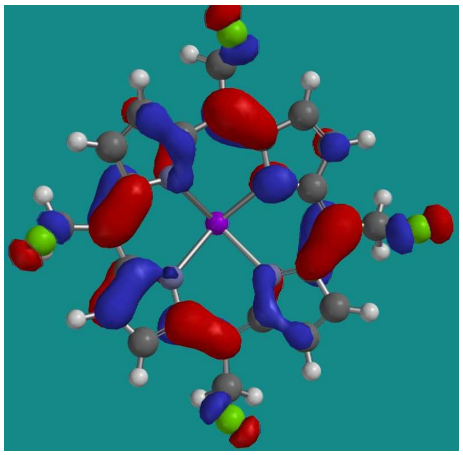

LUMO orbitals of compound **6**

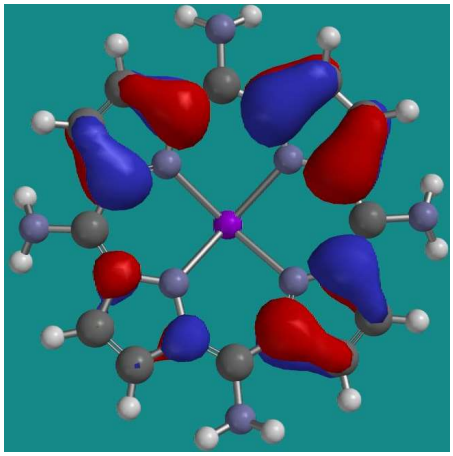

HOMO orbitals of compound **7**

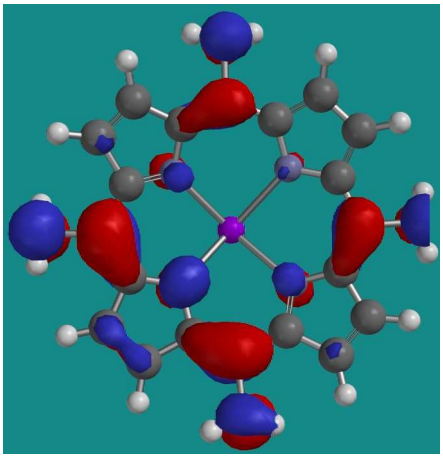

LUMO orbitals of compound **7**

Figure 4. Graphic representation of the frontier molecular orbitals of compounds **5**–**7**.

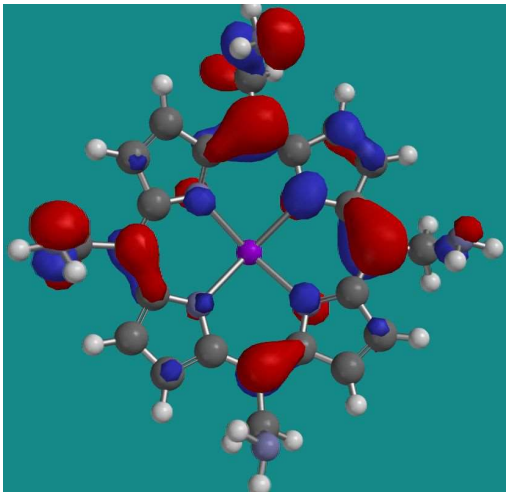

HOMO orbitals of compound **8**

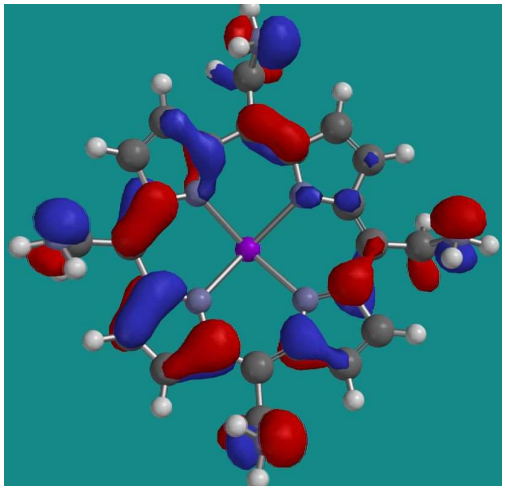

LUMO orbitals of compound **8**

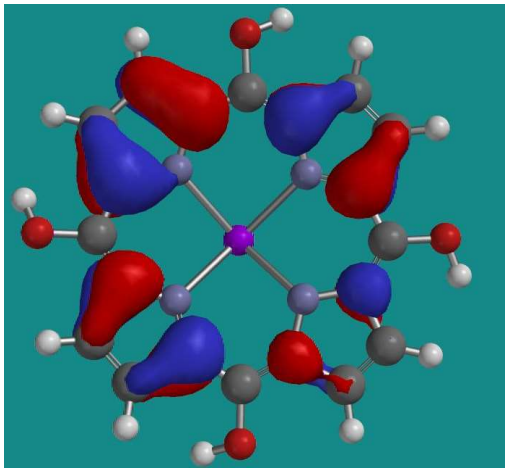

HOMO orbitals of compound **9**

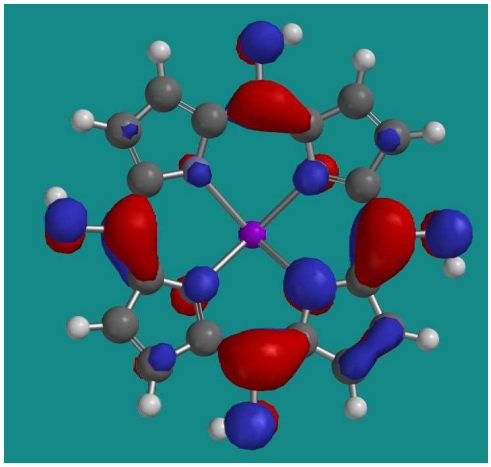

LUMO orbitals of compound **9**

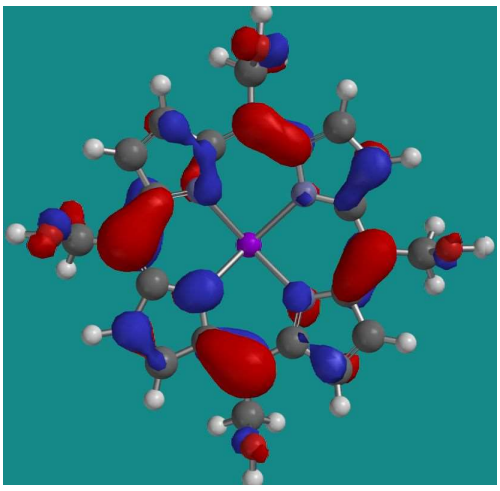

HOMO orbitals of compound **10**

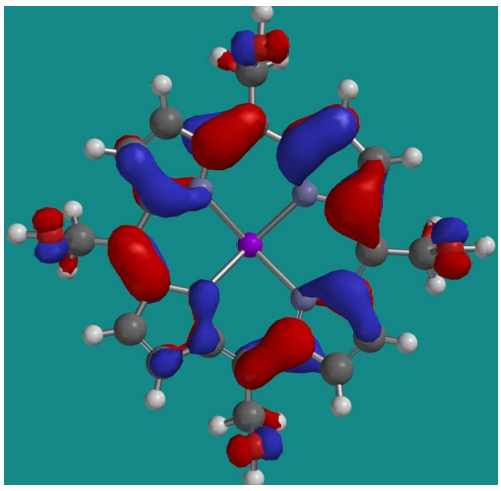

LUMO orbitals of compound 10

Figure 5. Graphic representation of the frontier molecular orbitals of compounds **8**–**10**.

The steric and geometric properties of the proposed Dy-porphyrins have also been calculated (**Table 3**). Steric properties like the molecular surface and volume provide a way to visualize the shape and size of molecules, aiding in understanding their overall structure. They are also used in virtual screening of potential drug candidates, assessing surface similarity and complementarity to target molecules.

Table 3. Steric parameters of the compounds (EDF2/6-31+G(d)).

Compound	Molecular area (Å²)	Molecular volume (Å³)	Ovality
1	329.54	327.16	1.44
2	393.78	398.20	1.50
3	352.03	347.15	1.47
4	416.14	417.11	1.54
5	383.86	381.99	1.51
6	460.53	455.34	1.61
7	373.54	369.21	1.50
8	450.77	442.91	1.60
9	360.67	356.94	1.48
10	432.76	428.44	1.57

The analysis of these parameters shows, as expected, larger values for the -CH_2X-substituted compounds (compared to the X-substituted ones). Larger values for these parameters have been obtained for chloromethyl- (**6**), aminomethyl- (**8**), and hydroxymethyl- (**10**) Dy-porphyrins. The same compounds—**6**, **8**, and **10**—are characterized by the highest ovality, a steric parameter that measures the deviation from the spherical shape of a compound.

Polar surface area (PSA) is a molecular descriptor employed in medicinal chemistry, especially for predicting how well a molecule will pass through cell membranes. It represents the combined surface area of all polar atoms (mainly oxygen and nitrogen, including their attached hydrogen atoms) within a molecule [15]. PSA is a key parameter for assessing a drug's ability to be absorbed; molecules with a PSA above 140 Å² generally have poor membrane permeability, making them less likely to be absorbed effectively [16]. For molecules to cross the blood–brain barrier, a PSA below 60 Å² is generally preferred [16]. Polarizability represents the tendency of a molecule's electron cloud to distort in response to an electric field. This distortion results in an induced electric dipole moment. The degree of polarizability is strongly influenced by the number of electrons and the size of the molecule. It also plays a key role in determining the strength of intermolecular interactions.

The results depicted in **Table 4** show that the polar surface area of the investigated compounds is found to be within the range 17–120 Å². A significant increase is obtained for compounds **7**–**10**, the ones that bear hydroxyl and amino groups.

Table 4. Polar surface area (PSA), dipole moment, and polarizability of the Dy-porphyrins (EDF2/6-31+G(d)).

Compound	Polar surface area (Å²)	Dipole moment (D)	Polarizability
1	17.667	2.16	67.86
2	17.825	3.29	73.55
3	18.290	8.12	69.38
4	17.838	12.39	75.08
5	17.877	7.56	72.21
6	18.452	10.04	78.19
7	107.692	4.82	70.98
8	118.338	8.66	77.20
9	90.246	4.39	70.07
10	98.811	11.95	76.00

The analysis of the influence of substituents on the geometric properties of the Dy-porphyrins also dealt with the length measurements of the Dy-N bonds. The results are depicted in **Table 5**, while the numbering of the atoms involved is presented in **Figure 6**.

Table 5. Bond lengths for N(sp3)-Dy (atoms N1 and N3) and N(sp2)-Dy (atoms N2 and N4).

Compound	d(N1-Dy) (Å)	d(N2-Dy) (Å)	d(N3-Dy) (Å)	d(N4-Dy) (Å)
1	2.408	2.398	2.398	2.398
2	2.403	2.399	2.401	2.399
3	2.440	2.425	2.431	2.425
4	2.406	2.399	2.402	2.399
5	2.407	2.398	2.401	2.398
6	2.442	2.427	2.430	2.427
7	2.436	2.421	2.437	2.422
8	2.439	2.426	2.431	2.426
9	2.440	2.422	2.440	2.422
10	2.407	2.399	2.402	2.399

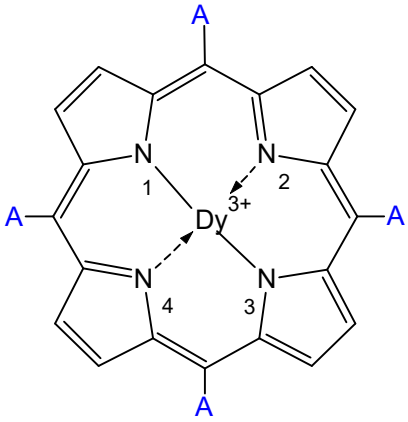

Figure 6. General structure of the Dy-porphyrins.

Also, taking into account the non-planar structure of the Dy-porphyrins (see the side-view depicted in **Figure 7**), the values of the angles formed by the nitrogen atoms and dysprosium have been determined.

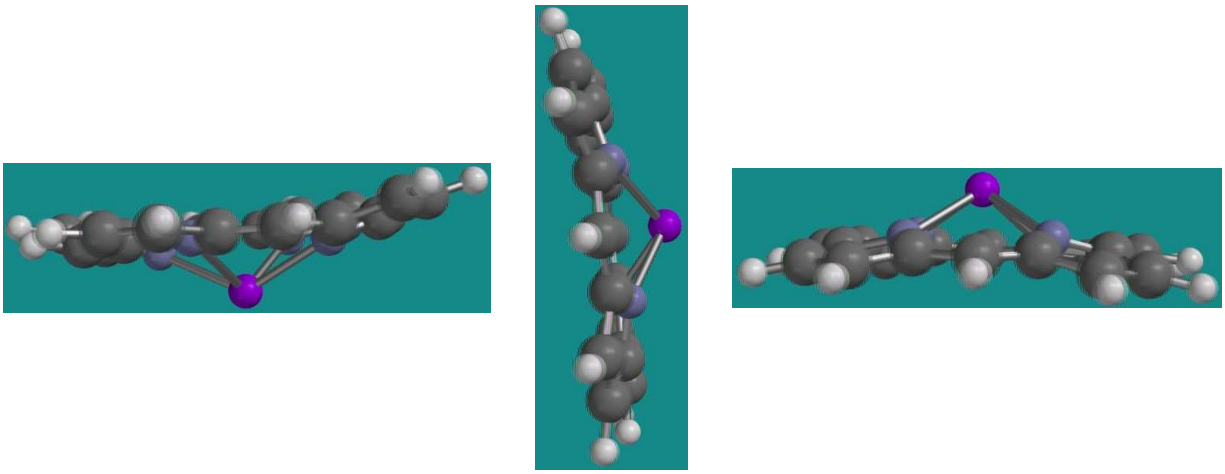

Figure 7. Side-view of the unsubstituted Dy-porphyrin 1 (similar for all the compounds within the series).

4. Conclusions

The present study analyzed the geometric and electronic properties of some Dy-porphyrins, substituted with various groups. The results showed that, according to the computed HOMO-LUMO gap, the most stable are compounds **7** and **9**,

the porphyrins bearing amino and hydroxyl groups. The above-mentioned compounds are characterized by bond lengths of approximately 2.44 Å for Dy-N(sp3) and 2.42 Å for Dy-N(sp2).

Considering the calculated energy per atom of the compounds within the series, the substitution with atoms leads to an increase in this parameter, together with the increase in the atomic number of the substituting atoms. The highest values have been obtained for chlorine -Cl, followed by fluorine –F, hydroxyl –OH, and amino –NH2. The presence of the CH2 group in compounds **4**, **6**, **8**, and **10** leads to a decrease in the total energy.

The frontier molecular orbital energies HOMO and LUMO are correlated with their symmetrical or unsymmetrical distribution (see compounds **7** and **8**).

According to the general structure of the investigated Dy-porphyrins depicted in **Figure 7** and to the results presented in **Table 6**, most of the proposed structures are characterized by the values of the angles between the sp3 nitrogen atoms and Dy of ~125°, while the values of the angles between the sp2 nitrogen atoms and Dy are close to ~131°.

Table 6. Values of the angles N-Dy-N.

Compound	∢(*N1*–*Dy*–*N3*) (°)	∢(*N2*–*Dy*–*N4*) (°)
1	121.93	130.62
2	122.30	131.39
3	126.58	130.33
4	121.53	131.35
5	125.57	130.42
6	125.34	130.92
7	125.36	131.35
8	125.18	131.13
9	125.92	130.69
10	121.62	131.04

Funding

This research received no external funding.

Author contributions

Conceptualization, S.R., R.P., and C.Ș.; Methodology, S.R., R.P., and M.J.; Software, S.R., R.P., E.A., and M.M.; Validation, S.R., R.P., E.A., and M.M.; Formal Analysis, R.P. and C.Ș.; Data Curation, S.R., M.J., and E.A.; Writing—Original Draft Preparation, S.R. and R.P.; Writing—Review and Editing, M.M. and C.Ș.; Visualization, R.P. and C.Ș.; Supervision, C.Ș. All authors have read and agreed to the published version of the manuscript.

Conflicts of interest

The authors declare no conflicts of interest.

Data availability statement

The original contributions presented in the study are included within the article. Further questions can be directed to the corresponding author.

Institutional review board statement

Not applicable.

Additional information

Received: 2025-07-15
Accepted: 2025-09-11
Published: 2025-09-16

Publisher's note

The Journal of Experimental Pharmacology and Toxicology remains neutral with regard to jurisdictional claims in published maps and institutional affiliations. All claims expressed in this article are solely those of the authors and do not necessarily represent those of their affiliated organizations, or those of the publisher, the editors, and the reviewers. Any product that may be evaluated in this article, or claim that may be made by its manufacturer, is not guaranteed or endorsed by the publisher.

Copyright

© 2025 copyright by the authors. This article is an open access article distributed under the terms and conditions of the Creative Commons Attribution (CC BY) license (https://creativecommons.org/licenses/by/4.0/).

References

1. Faustova M, Nikolskaya E, Sokol M, Fomicheva M, Petrov R, Yabbarov N. Metalloporphyrins in medicine: from history to recent trends. ACS Appl Bio Mater. 2020;3(12):8146–71. doi: 10.1021/acsabm.0c00941
2. Chandra R, Tiwari M, Kaur P, Sharma M, Jain R, Dass S. Metalloporphyrins-applications and clinical significance. Indian J Clin Biochem. 2000;15(Suppl. S1):183–99. doi: 10.1007/BF02867558
3. Schulz S, Wong RJ, Vreman HJ, Stevenson DK. Metalloporphyrins—an update. Front Pharmacol. 2012;3:68. doi: 10.3389/fphar.2012.00068
4. Stevenson DK, Wong RJ. Metalloporphyrins in the management of neonatal hyperbilirubinemia. Semin Fetal Neonatal Med. 2010;15(3):164–8. doi: 10.1016/j.siny.2009.11.004
5. Sullivan MV, Nanalal S, Dean BE, Turner NW. Molecularly imprinted polymer hydrogel sheets with metalloporphyrin-incorporated molecular recognition sites for protein capture. Talanta. 2024;266:125083. doi: 10.1016/j.talanta.2023
6. Guo YX, Liu B, Wang WL, Kang J, Chen JH, Sun WM. Computational screening of metalloporphyrin-based drug carriers for antitumor drug 5-fluorouracil. J Mol Graph Model. 2023;125:108617. doi: 10.1016/j.jmgm.2023.108617
7. Mkacher H, Taheur FB, Amiri N, Almahri A, Loiseau F, Molton F, et al. DMAP and HMTA manganese(III) meso-tetraphenylporphyrin-based coordination complexes: Syntheses, physicochemical properties, structural and biological activities. Inorganica Chim Acta. 2023;545:121278. doi: 10.1016/j.ica.2022.121278
8. Zhang Q, Yu W, Liu Z, Li H, Liu Y, Liu X, et al. Design, synthesis, antitumor activity and ct-DNA binding study of photosensitive drugs based on porphyrin framework. Int J Biol Macromol. 2023;230:123147. doi: 10.1016/j.ijbiomac.2023.123147
9. Király N, Zeleňák V, Lenártová N, Zeleňáková A, Čižmár E, Almáši M, et al. Novel Lanthanide(III) porphyrin-based metal-organic frameworks: structure, gas adsorption, and magnetic properties. ACS Omega. 2021;6(38):24637–49. doi: 10.1021/acsomega.1c03327
10. Zhao H, Zang L, Guo C. Influence of lanthanide ion energy levels on luminescence of corresponding metalloporphyrins. Phys Chem Chem Phys. 2017;19:7728–32. doi: 10.1039/C7CP00370F
11. Imran M, Ramzan M, Qureshi AK, Khan MA, Tariq M. Emerging applications of porphyrins and metalloporphyrins in biomedicine and diagnostic magnetic resonance imaging. Biosensors. 2018;8(4):95. doi: 10.3390/bios8040095
12. Kabiri S, Rahimi R, Mozafari MR, Naghib SM. Porphyrin-based metal–organic frameworks in drug delivery for cancer therapy: promises, advances and prospects. Discov Appl Sci. 2025;7:313. doi: 10.1007/s42452-025-06712-z
13. Pop R, Medeleanu M. Docking studies of porphyrin-based photosensitizers on rhombellanes. Croat Chem Acta. 2020;93(4):329–37. doi: 10.5562/cca3789
14. Spartan'14. Irvine (CA): Wavefunction Inc.; 2014.
15. Prasanna S, Doerksen RJ. Topological polar surface area: a useful descriptor in 2D-QSAR. Curr Med Chem. 2009;16(1):21–41. doi: 10.2174/092986709787002817
16. Global Antibiotic Research and Development Partnership (GARDP). Revive. [accessed on 1 Jun 2025]. Available from: https://revive.gardp.org/resource/polar-surface-area-psa/?cf=encyclopaedia